



**HAL**  
open science

## Structural Properties and Photocatalytic Activity of TiO<sub>2</sub> /Au Nanocomposites Synthesized with Glucose

Olena M Lavrynenko, Maksym M Zahornyi, Olesya Y Pavlenko, Claire Hotton, Jennifer Bodin, Vien-Duong Quach, Mohamed Nawfal Ghazzal, Erwan Paineau

► **To cite this version:**

Olena M Lavrynenko, Maksym M Zahornyi, Olesya Y Pavlenko, Claire Hotton, Jennifer Bodin, et al.. Structural Properties and Photocatalytic Activity of TiO<sub>2</sub> /Au Nanocomposites Synthesized with Glucose. *Particle & Particle Systems Characterization*, 2024, 41, pp.2400028. 10.1002/ppsc.202400028 . hal-04731712

**HAL Id: hal-04731712**

**<https://hal.science/hal-04731712v1>**

Submitted on 11 Oct 2024

**HAL** is a multi-disciplinary open access archive for the deposit and dissemination of scientific research documents, whether they are published or not. The documents may come from teaching and research institutions in France or abroad, or from public or private research centers.

L'archive ouverte pluridisciplinaire **HAL**, est destinée au dépôt et à la diffusion de documents scientifiques de niveau recherche, publiés ou non, émanant des établissements d'enseignement et de recherche français ou étrangers, des laboratoires publics ou privés.

**Structural Properties and Photocatalytic Activity of TiO<sub>2</sub>/Au Nanocomposites  
Synthesized with Glucose**

*Olena M. Lavrynenko,\* Maksym M. Zahornyi,\* Olesya Y. Pavlenko, C. Hotton, Jennifer Bodin, Vien-Duong Quach, Mohamed Nawfal Ghazzal, and Erwan Paineau\**

Dr. O. M. Lavrynenko, Dr. M. M. Zahornyi, Dr. O. Y. Pavlenko  
Frantsevich Institute for Problems of Materials Science NASU, 3 Omeliana Pritsaka Str.,  
Kyiv 03142, Ukraine  
E-mail: alena.lavrynenko@gmail.com; m.zahornyi@ipms.kyiv.ua

Dr. O. M. Lavrynenko, Dr. C. Hotton, J. Bodin, Dr. E. Paineau  
CNRS, Laboratoire de Physique des Solides, Université Paris-Saclay, Orsay 91405, France  
E-mail: erwan-nicolas.paineau@universite-paris-saclay.fr

V.D. Quach, Prof. M. N. Ghazzal  
CNRS, Institut de Chimie Physique, Université Paris-Saclay, Orsay 91405, France

Keywords: titanium dioxide, noble metals, glucose reduction, band-gap, dye degradation

A one-pot synthesis of plasmonic gold-modified TiO<sub>2</sub> nanocomposites is reported by using glucose reduction of HAuCl<sub>4</sub> in presence of titanium tetraisopropoxide. The resulting nanocomposites are characterized by thermal-gravimetric analyses, X-ray diffraction combined with X-ray fluorescence and photoelectron spectroscopies. A binary system of  $\beta$ -TiO<sub>2</sub> and anatase phases is obtained for low Au content while only anatase form is favored when the initial Au rate rises. This investigation also suggests the inclusion of gold in the TiO<sub>2</sub> structure. Although the optical band-gap of the different nanocomposites remains around 3 eV, the increase of Au content induces a shift of both valence and conduction edge bands to lower energy levels. The photocatalytic activity of TiO<sub>2</sub>/Au nanocomposites is assessed through the decolorization of different cationic and anionic dyes as model compounds. Regarding rhodamine and methylene blue dyes, the sample TiO<sub>2</sub> modified with 3.5 wt% of Au presents the best performance. The relation between the structure of the nanocomposites and their capacity to degrade pollutants is discussed.

## 1. Introduction

Titanium dioxide is one of the most studied oxides due to its numerous properties in terms of stability, optical transparency, abundance, and easy production. Since the pioneering work of Kawai and Sakata,<sup>[1]</sup> photocatalysts based on TiO<sub>2</sub> are used in various applications, including catalysis, energy conversion and storage or environmental remediation.<sup>[2–5]</sup> Among the polymorphs of TiO<sub>2</sub>, anatase is the most widely used for photocatalyst applications, one of the most famous products being Degussa (Evonik) P25.<sup>[6]</sup> However, the composition of the latter includes an admixture of rutile, which exhibits lower photocatalytic activity than anatase form.<sup>[7,8]</sup> A review of the modern scientific literature clearly indicates increased attention to the study of the catalytic activity of binary and ternary mixtures of TiO<sub>2</sub> polymorphs, which offer high degradation efficiency.<sup>[9]</sup> The well-known drawback of catalysts based on homogeneous TiO<sub>2</sub> phases is the high rate of electron and hole recombination, which reduces quantum efficiency and limits photocatalytic activity.<sup>[10]</sup> The use of a mixture of TiO<sub>2</sub> polymorphs enables a synergistic effect to be achieved thanks to the charge transfer generated between the different levels of their electronic bands.

While the anatase-rutile binary system is the most widely studied, other binary systems such as anatase/brookite<sup>[11]</sup> and anatase/ $\beta$ -TiO<sub>2</sub><sup>[12]</sup> as well as the ternary anatase/rutile/ $\beta$ -TiO<sub>2</sub> system<sup>[13]</sup> are less well known.  $\beta$ -TiO<sub>2</sub> (monoclinic structure), discovered in 1980, is even less studied. According to published data, its crystallization in aqueous media occurs in the presence of sodium cations, as  $\beta$ -TiO<sub>2</sub> has a covalent structure hosting bronze Na<sub>x</sub>TiO<sub>2</sub>.<sup>[14]</sup> Another way to increase the photocatalytic activity of titanium dioxide nanostructures is the coupling with noble metals. In particular, the introduction of gold into the system gives titanium dioxide particles plasmonic properties that enhance their photocatalytic activity and oxidative properties.<sup>[15,16]</sup> Several methods have been proposed during the last decades, such as a two-step (formation of TiO<sub>2</sub> nanoparticles followed by noble-metal deposition) or one-step process (co-condensation of the precursors prior to calcination).<sup>[17]</sup> We recently studied the impact of noble metal's deposition (Au, Ag, Pt or Pd) on the formation of TiO<sub>2</sub> nanoparticles synthesized from titanium tetraisopropoxide (TTIP) precursor. We showed differences in the structure, chemical and phase composition of the resulting nanocomposites.<sup>[18–20]</sup> It was found that the nature of noble metals may change not only temperature of phase transformation but the composition of reaction products as well. Alkali solutions, typically NaOH, are usually used as nucleating and reducing agents of the precursors. In this context, Mayya et al. proposed that the reduction of aqueous chloroaurate ions can be simply achieved in presence of glucose to form Au nanoparticles.<sup>[21]</sup> However, the use of glucose as a reducing agent for the direct synthesis of

gold-doped TiO<sub>2</sub> has been scarcely explored. To the best of our knowledge, only Nyamukamba et al. introduced glucose as a source of carbon to prepare Au/C co-doped TiO<sub>2</sub> nanocomposites.<sup>[22]</sup>

In this study, we aim at exploring the physical, chemical and structural characteristics of novel Au-modified TiO<sub>2</sub> structures formed in the presence of glucose. The resulting nanocomposites have been thoroughly characterized to determine their composition, structure and optical activity depending on the initial Au content. Although the band-gap of the resulting nanocomposites is found around 3 eV, the position of both conduction and valence band edges are slightly shifted to lower energies with increasing the Au content. Finally, the sorption and photocatalytic activities of the compounds have been tested for the degradation of different cationic and anionic dyes.

## 2. Results and discussion

### 2.1. Synthesis of TiO<sub>2</sub>/Au nanocomposites with glucose

The synthesis of TiO<sub>2</sub> nanocomposites is carried out by co-precipitation of water-ethanol solutions of titanium tetraisopropoxide (TTIP) and chloroauric acid HAuCl<sub>4</sub> in the presence of D-glucose (C<sub>6</sub>H<sub>12</sub>O<sub>6</sub>) as a reducing agent, urea (CH<sub>4</sub>N<sub>2</sub>O) as a hydrolysis regulator, NaOH as a nucleating agent, and ammonia solution to achieve a slightly alkaline environment (pH = 8.5-9). The initial amount of gold is varied between 0.5 and 3.5 wt.%. The resulting precipitates are washed with water and ethanol solutions and then lyophilized. Thermal gravimetric analysis of the precipitates was performed in the temperature range 20-1000 °C. **Figure S1** shows the curves related to thermal transformation of titanium-bearing precipitates prepared with 0.5 and 3.5 wt.% of Au. For a low Au amount, the DTG curve displays two main weight loss at 130°C and 440°C that correspond to adsorbed-binding water and destruction of TTIP, respectively. The total mass loss is equal to 33.9 %. The endotherm observed at 140 °C in the DTA curve may be related to the hydrolysis of TTIP and the early stage of the nucleation of titanium oxide phase. The wide shoulder in the range of 310-440 °C in DTA curve points to the destruction of TTIP and combustion of the organic components. It will be noted that brookite and anatase correspond to the low temperature polymorphs of TiO<sub>2</sub> that are completely crystallized at temperatures lower than 460 °C whereas the rutile phase is grown in the temperature range 790-950 °C. The increase in gold concentration to 3.5 wt% in the precipitate leads to a similar TGA curve with the remove of adsorbed water at 110 °C and the transformation of isopropoxide components around 460 °C. However, a third weight loss is observed at 230°C, which can be related to the dehydroxylation of Au(OH)<sub>3</sub> and the formation of Au<sub>2</sub>O<sub>3</sub> oxide. The reduction of

this gold oxide may lead to reduce gold clusters on the TiO<sub>2</sub> surface or the inclusion of Au in the crystal lattice of TiO<sub>2</sub>. Based on these results, we prepared different TiO<sub>2</sub> nanocomposites with varying amount of Au (referred hereafter as TiO<sub>2</sub>/Au\_X (with X the initial amount of gold in wt%)) by calcination the precipitate at 600°C during 2 h.

## 2.2. Morphology and structure of the nanocomposites

The phase composition of the resulting nanocomposites is studied first by X-ray diffraction (XRD). **Figure 1** displays the powder X-ray diffractograms of the different TiO<sub>2</sub>/Au nanocomposites. The thermal treatment at 600°C leads to the formation of different TiO<sub>2</sub> compounds depending on the initial Au content.

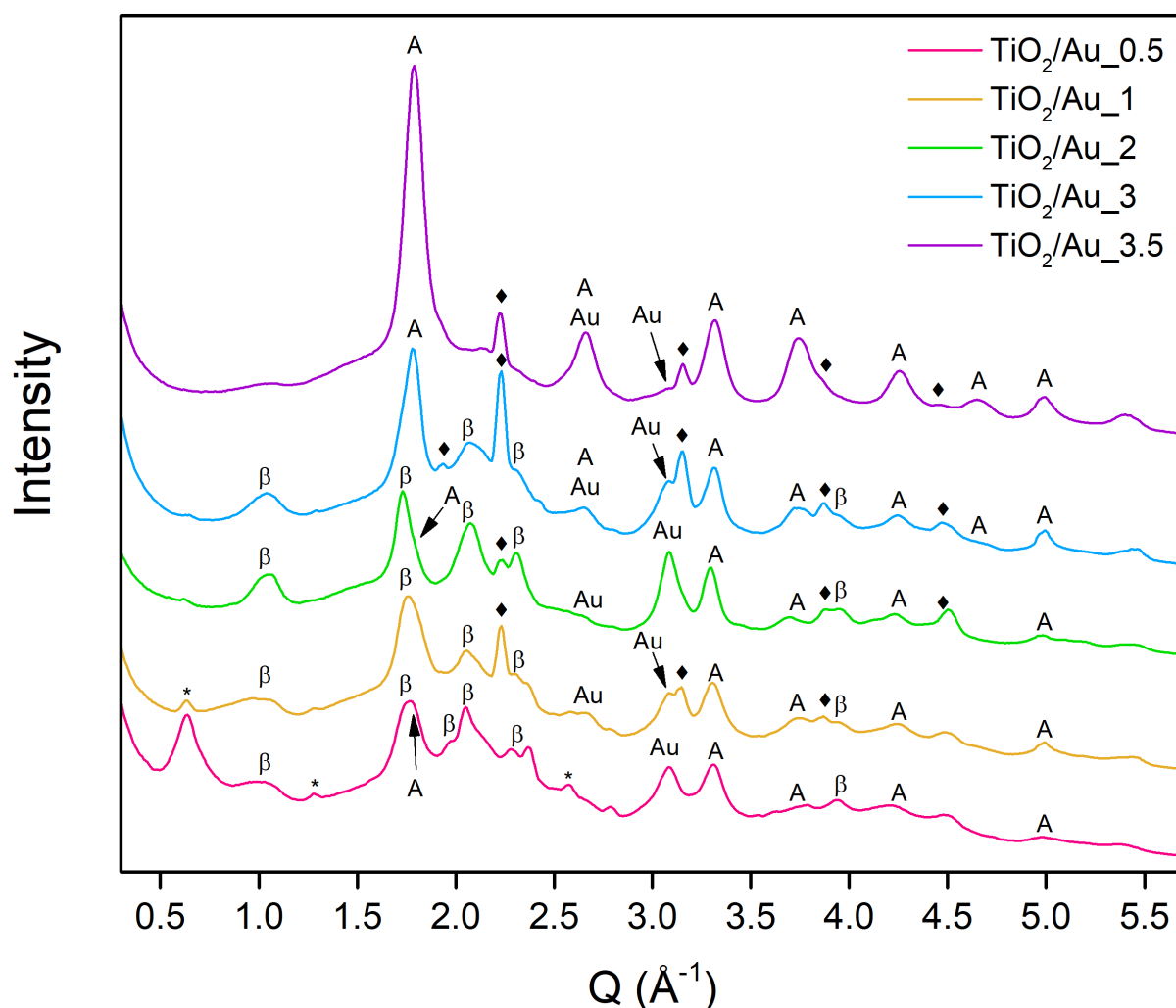


**Figure 1.** XRD diffractograms of the different TiO<sub>2</sub>/Au nanocomposites. The labels correspond to the main reflections of the different phases: A- anatase;  $\beta$  –  $\beta$ -TiO<sub>2</sub>; Au – gold. Diamonds and stars are related to residual NaCl salt and a parasitic Ti phase (see text), respectively.

For TiO<sub>2</sub>/Au\_0.5, the sample is mainly composed of the  $\beta$ -TiO<sub>2</sub> phase. The characteristic peaks of the crystalline anatase phase are also observed, indicating that the sample contains mixed phases of  $\beta$ -TiO<sub>2</sub> and anatase. We also notice additional peaks at  $Q = 0.6, 1.2$  and  $2.5 \text{ \AA}^{-1}$ , whose

rationality suggests a two-dimensional lamellar Ti compound. However, both this lamellar phase and  $\beta$ -TiO<sub>2</sub> phase tend to be replaced by anatase with increasing the Au content, confirming that the latter is the most stable TiO<sub>2</sub> phase for calcination temperature around 600°C.<sup>[23]</sup> In addition, the presence of gold can be attested by the occurrence of several Bragg peaks as indexed in **Figure 1**. To identify the influence of Au reduction on TiO<sub>2</sub>, we have calculated the crystal lattice parameters and compared to standard sample of anatase (JSPDS No. 21-1272). The characteristic lattice parameters are summarized in **Table S1**. We evidence that the reduction of Au by glucose during the synthesis of TiO<sub>2</sub> induces a modification of *a* and *c* parameters. The tetragonality degree (*c/a*) of all the nanocomposites is always higher (2.55-2.64) than for standard anatase (2.51), suggesting the inclusion of Au cations in the TiO<sub>2</sub> structure during the reduction process. The position of the *d*-spacing of the (101) plane (at  $Q \sim 1.78 \text{ \AA}^{-1}$ ) is slightly shifted to higher values, pointing to a distortion of the crystal lattice in presence of Au.

The morphology of as-synthesized samples was assessed by scanning electron microscopy (SEM) and transmission electron microscopy (TEM) observations for the two outermost nanocomposites (**Figure S2**). In particular, based on TEM images, TiO<sub>2</sub>/Au\_0.5 displays small and slightly wrinkled particles, probably related to the predominant  $\beta$ -TiO<sub>2</sub> phase, while small rounded particles are observed for TiO<sub>2</sub>/Au\_3.5. However, the observations do not reveal the formation of gold nanoparticles on the surface, as it is often the case in co-deposition studies, but rather smooth surfaces. To confirm the reduction of gold in these nanocomposites, we perform X-ray fluorescence (XRF) spectroscopy (**Figure 2 and Figure S3**). The XRF spectra of both TiO<sub>2</sub>/Au\_0.5 and TiO<sub>2</sub>/Au\_3.5 nanocomposites display two peaks at around 9.7 and 11.4 keV that correspond to the Au L<sub>3</sub> and L<sub>2</sub> lines, respectively.

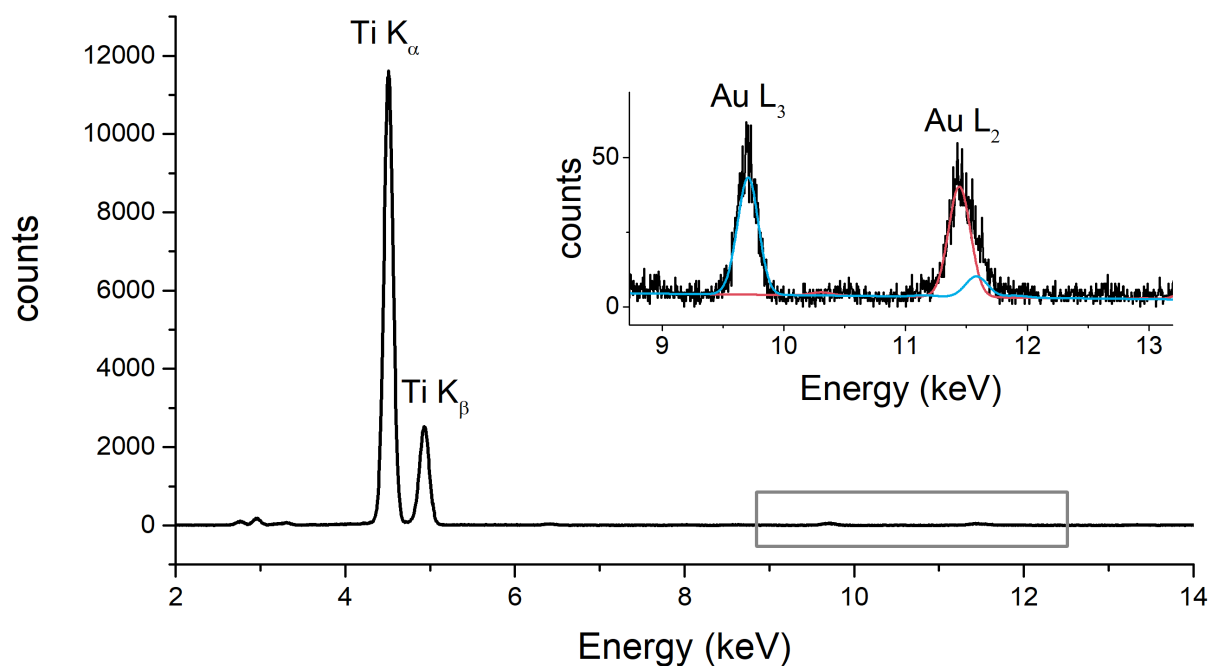


**Figure 2.** X-ray fluorescence spectra obtained on  $\text{TiO}_2/\text{Au}_{3.5}$  nanocomposite. Position of the  $\text{K}\alpha$  fluorescence peak of Ti is represented. The inset is a zoom of the grey rectangle, corresponding to the  $\text{L}_{3,2}$  fluorescence peak of gold (Au). The colored lines represent the fit of the Au contribution.

To go further, the chemical composition and oxidation states of the nanocomposites was analyzed by X-ray photoelectron spectroscopy (XPS). The survey spectra show the main contributions of Ti and O species (**Figure S4**) except for the Au  $4f$  signal that cannot be detected. It is also worth to note that XPS is a local probe compared to XRD and XRF. This suggests an inclusion of gold with a diffuse distribution into the  $\text{TiO}_2$  structure without the formation of metallic nanoparticles on the surface of  $\text{TiO}_2$  as shown by TEM observations. The high resolution XPS spectra of Ti 2p (**Figure 3a**) shows two sharp peaks with binding energies (BE) at 458.9 and 464.5 eV, corresponding to the two spin-orbit components  $2p_{3/2}$  and  $2p_{1/2}$ . The BE values and the separation between the spin-orbit components, close to 5.7 eV, are consistent with what is expected for  $\text{Ti}^{4+}$  in a  $\text{TiO}_2$  structure.<sup>[24,25]</sup> The deconvolution of the O 1s signal presents several contributions (**Figure 3b**). The main peak is found at 530.3 eV, which is assigned to Ti-O bond in the oxide. The curve-resolved of the O 1s contribution reveals a shoulder at 531.6 eV that is characteristic of surface hydroxyl in  $\text{TiO}_2$  compounds.<sup>[26]</sup> The contribution at higher BE corresponds to H-O from adsorbed water molecules on the nanocomposites surfaces. We also noticed a shift of the binding energy position of Ti and O contribution for the highest Au content nanocomposite. However, this sample contains only

anatase TiO<sub>2</sub> polymorph compared to the others, which may explain the difference in the XPS spectra.

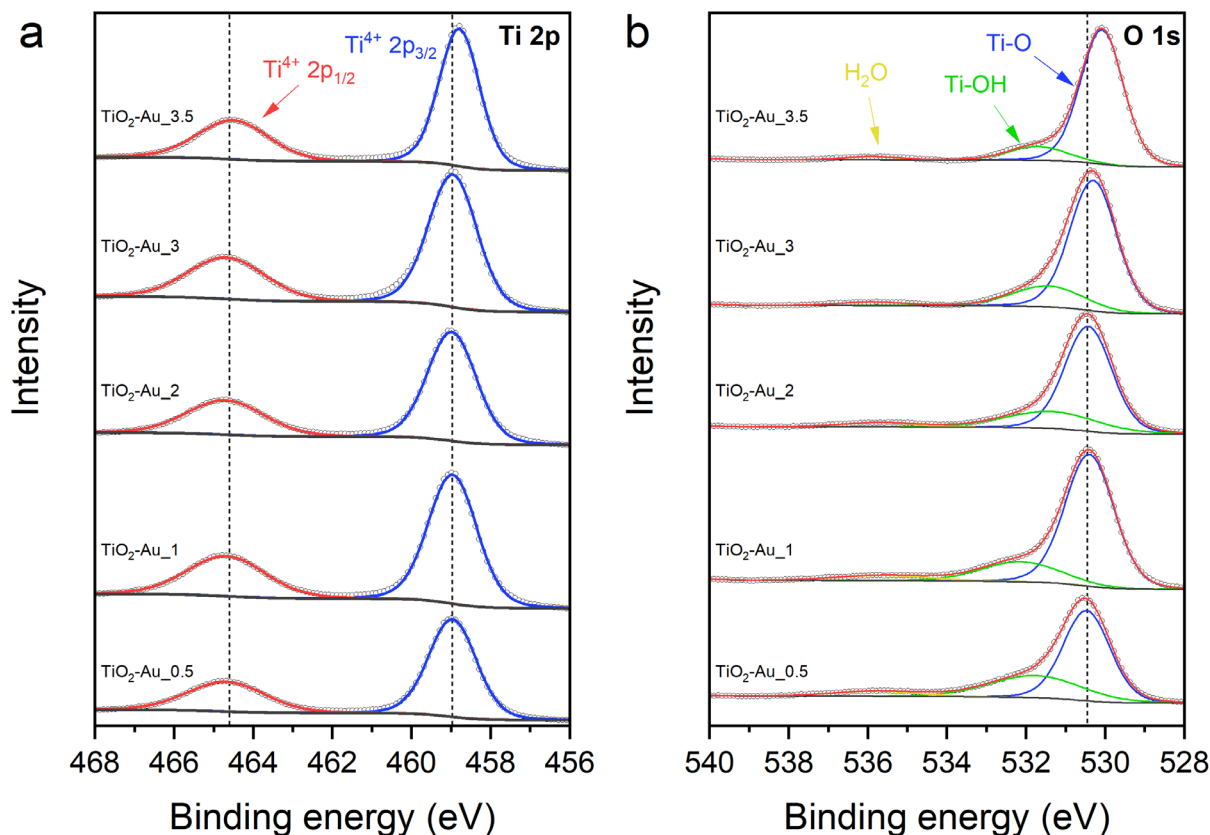


**Figure 3.** XPS spectra for (a) Ti 2p and (b) O 1s of the different TiO<sub>2</sub>/Au nanocomposites. The curves have been translated vertically for the sake of clarity.

### 2.3. Optical properties

The optical properties of the different TiO<sub>2</sub>/Au nanocomposites were characterized by ultraviolet/visible diffuse reflectance spectroscopy (DRS) (**Figure 4a**). The samples display an absorption in the UV range (< 350 nm), which is typical of the band-to-band transition of TiO<sub>2</sub>.<sup>[27]</sup> In addition, a clear maximum is observed around 550–600 nm. This corresponds to the surface plasmon resonance of Au in loose configuration,<sup>[28–30]</sup> thus validating the reduction and deposition of Au during the TiO<sub>2</sub> synthesis. The value of the bandgap energy ( $E_g$ ) is estimated from the corresponding Tauc plot by applying the Kubelka-Munk (K-M) theory (**Figure 4b**). The TiO<sub>2</sub>/Au nanocomposites exhibit a bandgap around  $3.05 \pm 0.04$  eV, whatever of the Au doping, which is slightly lower than that reported for pure anatase (3.2 eV).<sup>[7]</sup> The creation of an optical band gap in semiconductors is defined as the difference between the valence band edge (VBE) and conduction band edge (CBE). In order to determine the position of the VBE, we analyzed the high-resolution XPS spectra at low binding energy as illustrated in **Figure 4c**. Combined with the  $E_g$  values determined from DRS experiments, we report in **Figure 4d** the

energy diagram scheme as a function of the initial Au content in the nanocomposites. Although the bandgap changes only marginally, we observe that the position of the VBE (and consequently the CBE) varies significantly as a function of the Au doping level. Combined with the previous characterization results, we ascribe this effect to the incorporation of Au atoms into the TiO<sub>2</sub> structure, modifying the resulting optical properties of the nanocomposites.

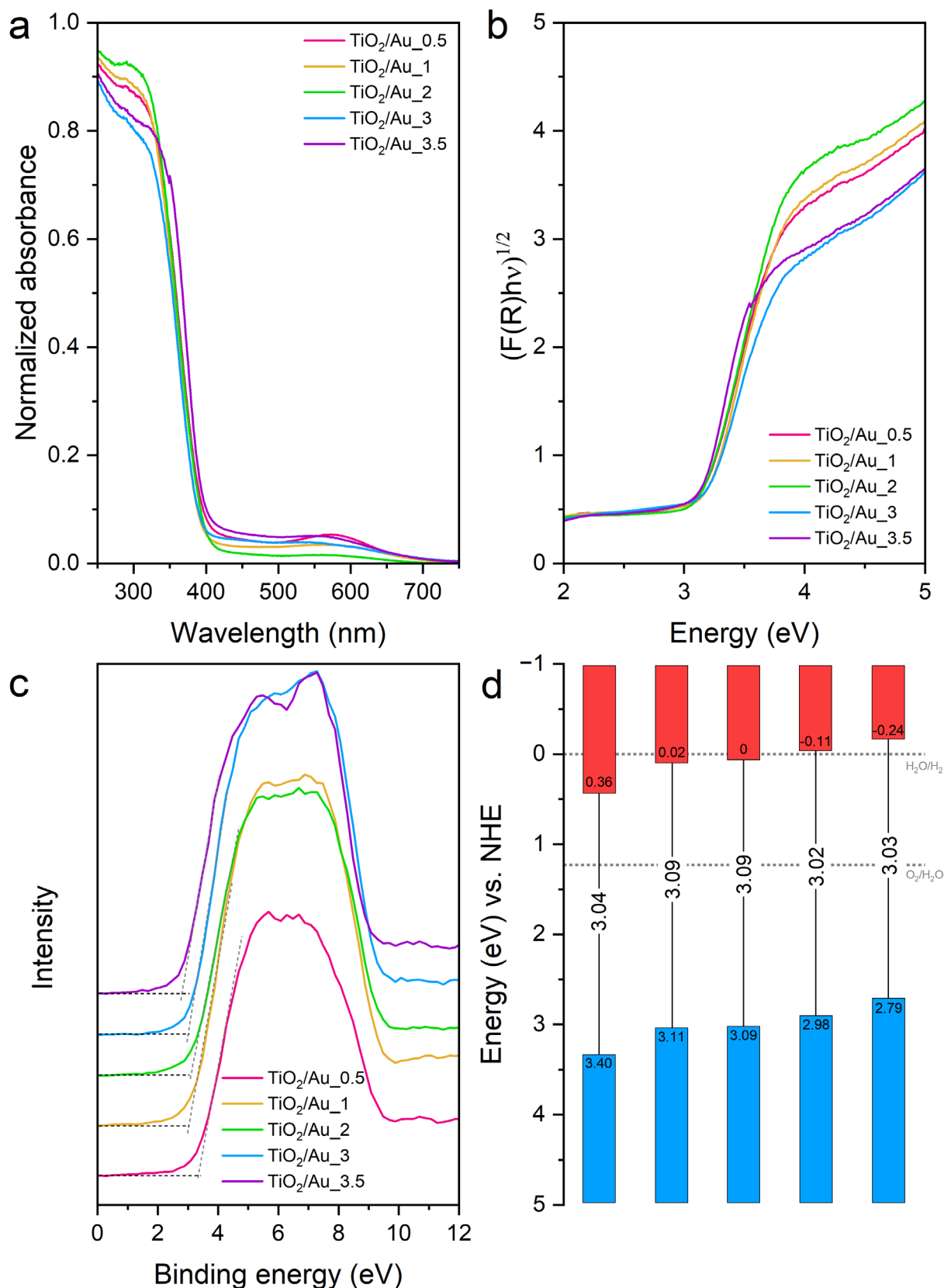


**Figure 4.** (a) Diffuse reflectance spectra and (b) their corresponding Tauc plots. (c) XPS spectra around the valence band region. (d) Energy diagram scheme of the different TiO<sub>2</sub>/Au nanocomposites as a function of the normal hydrogen electrode (NHE). The conduction and

valence bands are represented in red and blue, respectively. The corresponding bandgap values are reported in black.

#### 2.4. Decolorization of cationic and anionic dye solutions

The variation of the optical properties could have a direct effect on the photocatalytic performance of the TiO<sub>2</sub>/Au nanocomposites. To verify this point, we opted to test the different nanocomposites for the degradation of various model dyes. We selected four charged dyes (**Figure 5**), 3 cationic (Malachite green – MG; Methylene blue – MB; Rhodamine B – RhB) and one anionic (Orange G – OG).

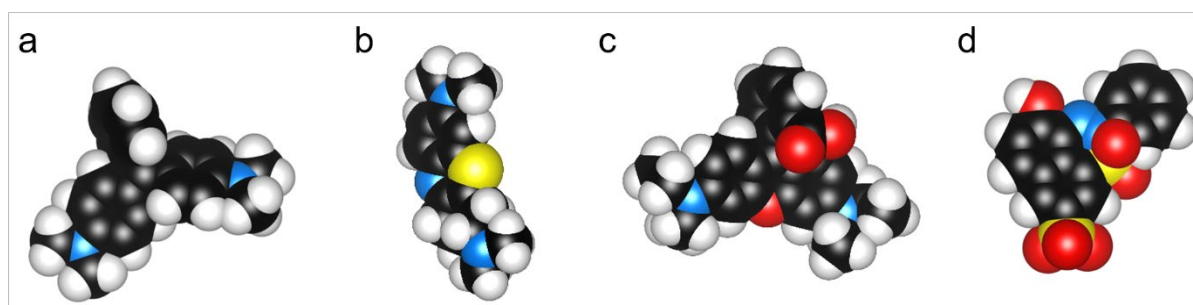


**Figure 5.** 3D representation of the different dye molecules used for photocatalytic degradation. (a) Malachite green (MG); (b) Methylene blue (MB); (c) Rhodamine B (RhB); (d) Orange G (OG). Color code of atoms: carbon (black), hydrogen (white), nitrogen (blue), sulfur (yellow), oxygen (red).

The photodegradation tests are performed by dispersing 50 mg of TiO<sub>2</sub>/Au nanocomposites in a glass filled with 50 mL of aqueous dye solution ( $C_0 = 20 \text{ mg.L}^{-1}$ ). Prior to experiments, the mixtures are stirred in the dark during 30 min to reach the adsorption-desorption equilibrium. Then, the mixtures are left to stir under visible light (VL) of the laboratory for 30 min, followed by an exposition under a UV-vis lamp for another 70 min, except for MG solutions that are constantly stirred under VL (see Method section for details). **Figure 6a** illustrates the UV-Vis spectra of MB solutions after 130 min of contact with the different TiO<sub>2</sub>/Au nanocomposites. Compared to the reference MB solution, we observe a strong decrease of the absorption bands at 660 and 610 nm related to the monomeric and dimeric species of MB molecules.<sup>[31]</sup> MB is a cationic dye, with the chromophore N-S conjugated system on the central aromatic heterocycle, and a decrease in band intensity indicates that the conjugated structure of the heterocycle is destroyed, especially after contact with the sample TiO<sub>2</sub>/Au\_3.5. **Figure 6b** illustrates the evolution of the decolorization as a function of the progress of the photodegradation test. After the dark step, an important part of the MB dye has been removed from the solution, which can be ascribed to adsorption on the nanocomposites. Nevertheless, the application of UV-visible

radiation improves the percentage of decolorization of solutions, reaching almost 100% for  $\text{TiO}_2/\text{Au}$  nanocomposites prepared with 3.5 wt% of Au.

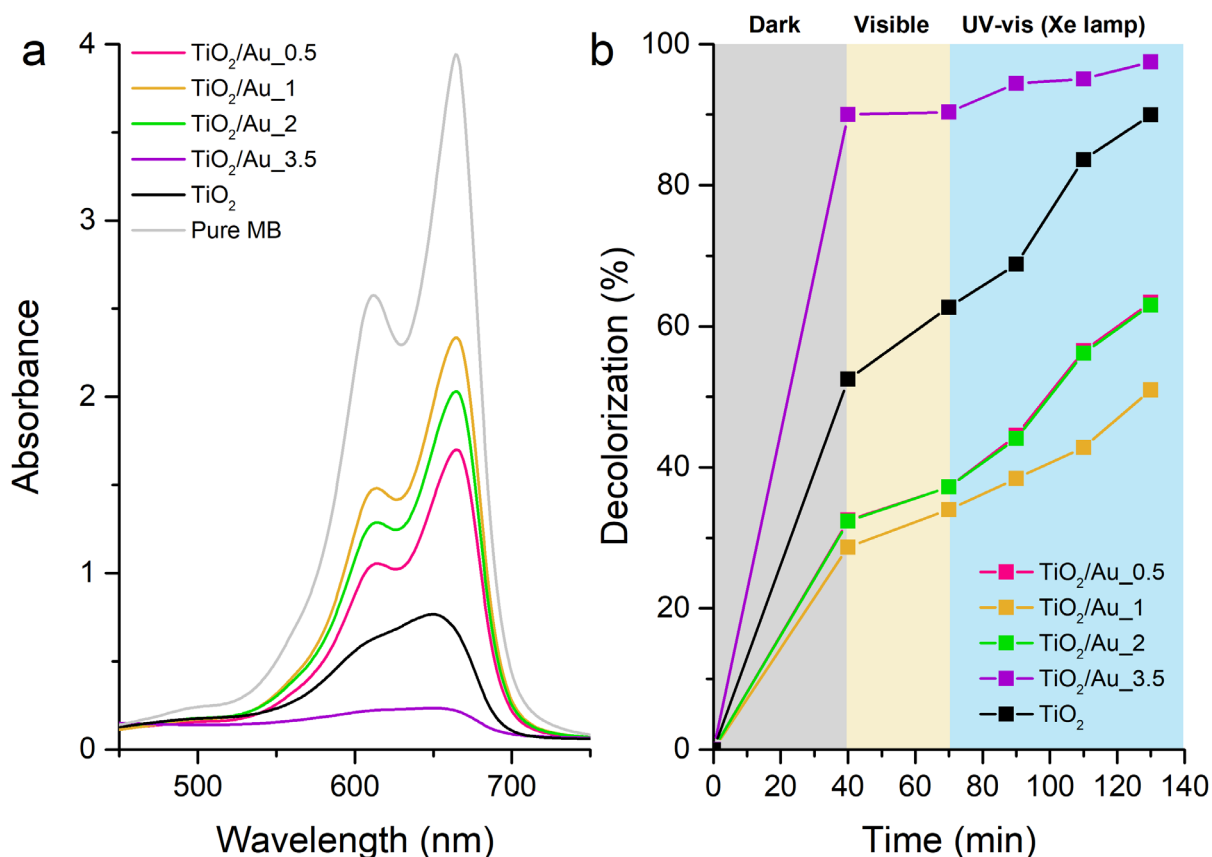


**Figure 6.** Photocatalytic activity of  $\text{TiO}_2/\text{Au}$  nanocomposites toward the removal of methylene blue dye solution. (a) UV-Vis spectra of the supernatant after 130 min of contact with the nanocomposites. Results with undoped  $\text{TiO}_2$  and pure MB suspension ( $20 \text{ mg}\cdot\text{L}^{-1}$ ) are provided for comparison. (b) Evolution of the decolorization of MB aqueous suspensions. The different steps of the photodegradation tests are highlighted.

We have performed similar experiments for the different dyes. **Figure 7** summarizes the residual dye concentrations after contact of the different nanocomposites with the dye solution during 130 minutes.

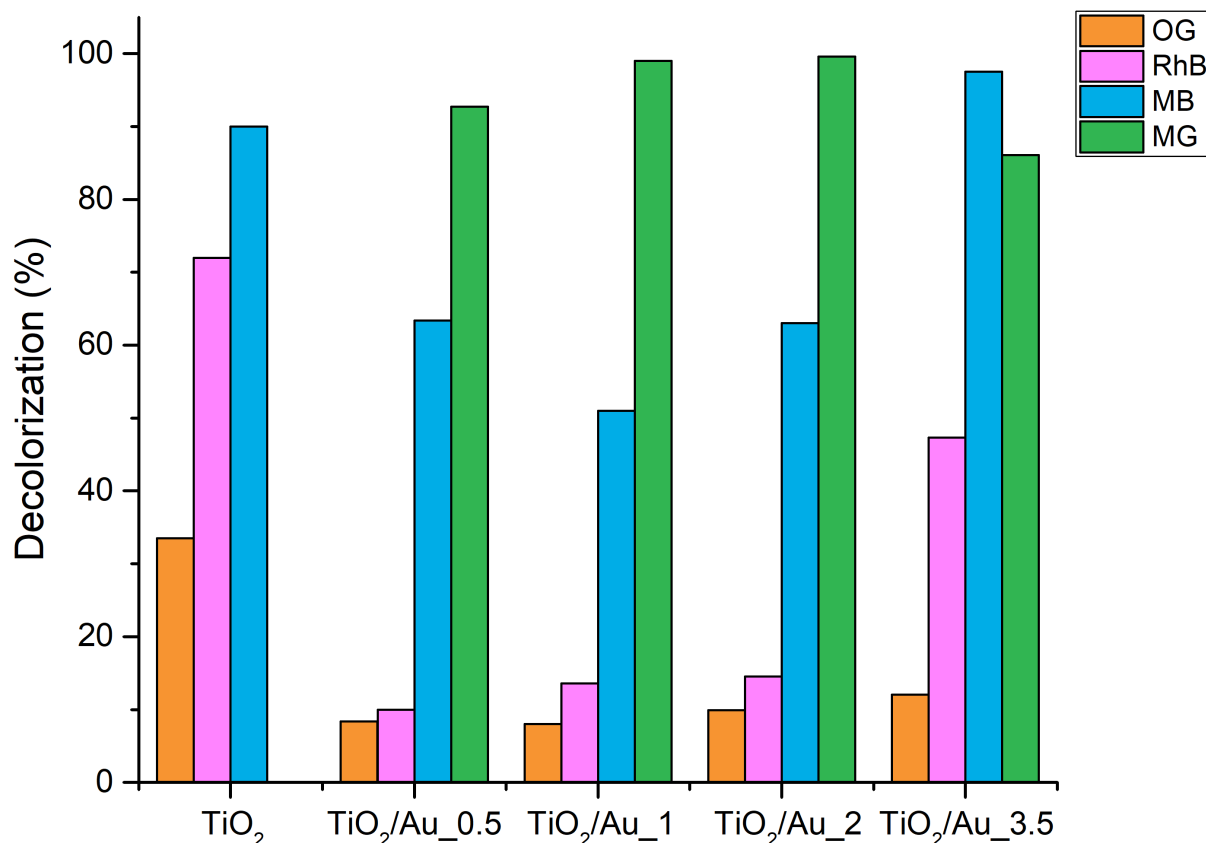


**Figure 7.** Photodegradation activity of the different catalysts as a function of the dye ( $20 \text{ mg}\cdot\text{L}^{-1}$ ) and after 130 min of contact.

This systematic study reveals contrasting effects depending on the nature of the dyes and the nanocomposite composition. In all cases, the anionic dye (OG) is the one that persists most easily in solution. It has little or no degradation (less than 15%) by the prepared TiO<sub>2</sub>/Au nanocomposites as well as by pure anatase TiO<sub>2</sub> (< 35%) in the present conditions. The TiO<sub>2</sub>/Au\_3.5 nanocomposite presents the best performance for decolorization of RhB and MB dyes solutions, with regards to lower Au doping samples. By contrast, MG is removed very efficiently by all nanocomposites, with a decolorization rate of around 90%, although slightly lower for TiO<sub>2</sub>/Au\_3.5. At the same time, all nanocomposites have a high sorption activity and, when in contact with MG solutions in the dark, are able to remove from the solution from 41 to 90% of the dye. The differences observed between the nanocomposites is related at the first order to the phase composition of the nanocomposites. As evidenced from XRD and TEM, nanocomposites prepared at a low Au content form a mixture of  $\beta$ -TiO<sub>2</sub> and anatase phases while anatase is the main TiO<sub>2</sub> phase for TiO<sub>2</sub>/Au\_3.5 that shows the best performance for dye degradation. Further work on the decolorization capacity of  $\beta$ -TiO<sub>2</sub> would be interesting but it goes beyond the scope of this study. Beyond these sample differences, the analysis of the

evolution of the decolorization for the different dye solutions indicates that the primary mechanism of dye extraction is its sorption from the solution. The second mechanism is probably a catalytic decomposition under the influence of UV-Vis radiation as evidenced by the modification of the shape of the UV-Vis spectra (**Figure 6a**).

### 3. Conclusion

In summary, the synthesis of Au-doped TiO<sub>2</sub> nanocomposites was carried out by a chemical co-deposition method using TTIP and HAuCl<sub>4</sub> in the presence of glucose used as reducing agent of gold. Both anatase and  $\beta$ -TiO<sub>2</sub> phases are formed at T = 600 °C for low Au content. The anatase form is favored when the initial Au rate rises. Structural characterizations confirm that Au is dispersed homogeneously into the nanocomposites. Investigations of the optical behavior reveal a slight decrease of the bandgap compared to pure anatase. More interestingly, the incorporation of Au into the resulting nanocomposite induces a progressive shift of both valence and conduction band edges, offering a straightforward approach to modify the band alignment of TiO<sub>2</sub> nanocomposites. Testing the photocatalytic activity under UV-Vis light conditions shows that the best performance is obtained for sample prepared with an initial Au content of 3.5 wt%. Although the main mechanism of dye extraction by these Au-doped TiO<sub>2</sub> nanocomposites is dye sorption, we also evidence a second mechanism by catalytic decomposition. The use of different dye molecules allows us identifying contrasting effects depending on the nature of the dyes, cationic dyes being better adsorb and/or degraded by the nanocomposites than anionic dye. Despite the fact that photodegradation performance may remain modest, we believe that the proposed approach offers interesting prospects for the development of improved gold-doped TiO<sub>2</sub> by the use of glucose as a green reducing agent.

### 4. Experimental section

*Thermal analyses:* Thermal-gravimetric and differential thermal analysis (TG-DTA) was carried out on a thermal analyzer Q-1500D (Hungary) under static air atmosphere. 150 mg of powder was placed into a corundum crucible and covered by a quartz beaker to create a homogenous temperature field. The samples were heated at a rate of 10 °C/min from 20 to 1000 °C.

*X-ray diffraction:* Powder X-ray diffraction experiments were carried out on a rotating anode generator (Rigaku Corp., Japan) operated at the Mo wavelength ( $\lambda = 0.0711$  nm). Powder samples were packed in borosilicate capillaries. Scattering patterns were collected on a MAR345 detector (marXperts GmBH, Germany) with 150  $\mu$ m pixel size placed behind the sample at a distance of 150 mm. Extraction of the scattered intensity  $I$  as a function of the scattering modulus  $Q$  ( $Q = 4\pi/\lambda \sin\theta$ , with  $2\theta$  the scattering angle) was performed with home-

developed software. The analysis of the XRD data was performed by the help of Maud program and International Powder Standards Committee (JSPDS International Centre for Diffraction Data 1999) database.

*X-ray fluorescence spectroscopy:* The measurements have been performed on an X-ray microsource generator (Incoatec I $\mu$ S Mo  $\lambda = 0.0711$  nm). A silicon drift diode detector (Ketec GmbH) assures fluorescence detection. Analysis of the XRF data was realized using PyMCA software.<sup>[32]</sup>

*Electron microscopy:* Scanning electron microscopy (SEM) was performed with a Zeiss Supra55VP and an acceleration voltage of 2 keV. The samples were placed on an UV treated silicon wafer. SEM images were acquired with SE2 detector. Transmission electron microscopy (TEM) was carried out on a JEOL1400 microscope operating at 120 kV. Powder samples were diluted in ethanol and a drop of this mixture was deposited on a copper grid coated with a carbon layer and dried at room temperature.

*Characterization of optical properties:* Optical properties were determined using diffuse reflectance spectroscopy on a UV-Vis spectrometer (model Cary 5000 series, Agilent Technologies) equipped with an integrating sphere. The maximum reflectance was set to 100% using BaSO<sub>4</sub> as a reference in a wavelength range between 200 to 800 nm. The X-ray photoelectron spectroscopy (XPS) measurements were performed on a K Alpha spectrometer from ThermoFisher, equipped with a monochromated X-ray Source (1486.6 eV) with a spot size of 400  $\mu$ m. The hemispherical analyzer was operated in CAE (Constant Analyzer Energy) mode. The charge build-up was neutralized by means of a “dual beam” flood gun. The obtained spectra were treated by means of the CasaXPS software.

*Photocatalytic tests:* The photocatalytic activity of Au-doped TiO<sub>2</sub> powders was assessed by following the removal of different dyes in aqueous solution. Three cationic dyes (Malachite Green (MG) – C<sub>23</sub>H<sub>25</sub>N<sub>2</sub>Cl; Methylene Blue (MB) – C<sub>13</sub>H<sub>18</sub>N<sub>3</sub>SCl; Rhodamine B (RhB) – C<sub>28</sub>H<sub>31</sub>N<sub>2</sub>O<sub>3</sub>Cl) and one anionic dye (Orange G (OG) - C<sub>16</sub>H<sub>10</sub>N<sub>2</sub>O<sub>7</sub>S<sub>2</sub>Na<sub>2</sub>) were dispersed at 20 mg.L<sup>-1</sup> in ultrapure water. 50 mg of TiO<sub>2</sub>/Au powder samples was placed in a glass filled with 50 mL of aqueous dye solution. The mixture was stirred in the dark for 30 min to reach the adsorption-desorption equilibrium. For MG, the suspensions were constantly stirred under visible light (VL) while for the other dyes, the suspensions were stirred during 30min under VL followed by illumination under UV-Vis with a Xe lamp (LOT Design, 15.5 mW.cm<sup>-2</sup>).<sup>[29]</sup> Aliquots were collected at various time that were filtered and centrifugated at 8g for 30 min. The resulting supernatant was analyzed by UV-vis spectroscopy (model Cary 5000 series,

Agilent Technologies) in transmission mode using polystyrene cuvettes with a 10 mm optical path length.

### Supporting Information

Additional characterizations are provided in Supporting Information available from the Wiley Online Library.

### Acknowledgements

The authors acknowledge the MORPHEUS platform (LPS, Orsay) for X-ray scattering and fluorescence experiments. We thank D. Dragoë for her help during XPS experiments and Dr. Claire Goldmann for TEM observations. Dr. O. M. Lavrynenko is supported by the PAUSE program, a national emergency program for scientists and artists in exile, run by the Collège de France. The results used the Imagerie-Gif core facility supported by l'Agence Nationale de la Recherche (ANR-11-EQPX-0029/Morphoscope, ANR-10-INBS-04/FranceBioImaging; ANR-11-IDEX-0003-02/ Saclay Plant Sciences).

Received: ((will be filled in by the editorial staff))

Revised: ((will be filled in by the editorial staff))

Published online: ((will be filled in by the editorial staff))

### References

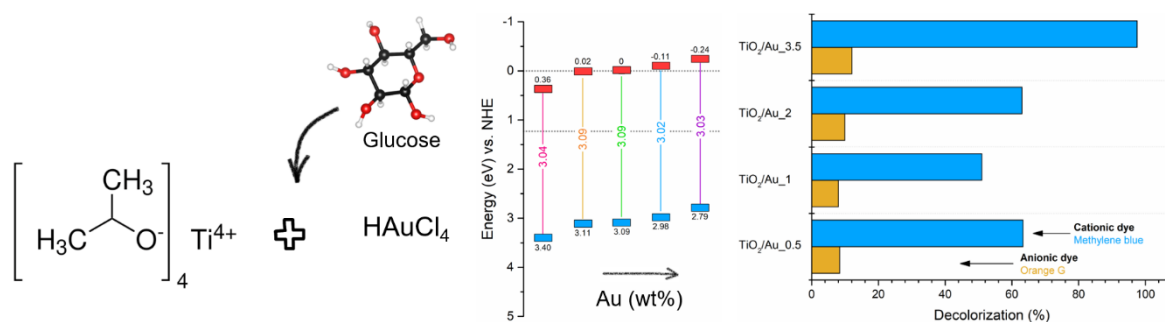
- [1] T. Kawai, T. Sakata, *J. Chem. Soc. Chem. Commun.* **1980**, 694–695.
- [2] W. Zhang, Y. Tian, H. He, L. Xu, W. Li, D. Zhao, *Natl. Sci. Rev.* **2020**, *7*, 1702–1725.
- [3] K. P. Gopinath, N. V. Madhav, A. Krishnan, R. Malolan, G. Rangarajan, *J. Environ. Manage.* **2020**, *270*, 110906.
- [4] M. Zahorny, G. Sokolsky, *Nanosized Titania Composites for Reinforcement of Photocatalysis and Photoelectrocatalysis*, Cambridge Scholars Publishing, **2022**.
- [5] C. Wang, M. N. Ghazzal, *Energy Adv.* **2023**.
- [6] B. Ohtani, O. O. Prieto-Mahaney, D. Li, R. Abe, *J. Photochem. Photobiol. Chem.* **2010**, *216*, 179–182.
- [7] J. Zhang, P. Zhou, J. Liu, J. Yu, *Phys. Chem. Chem. Phys.* **2014**, *16*, 20382–20386.
- [8] T. Luttrell, S. Halpegamage, J. Tao, A. Kramer, E. Sutter, M. Batzill, *Sci. Rep.* **2014**, *4*, 4043.
- [9] D. R. Eddy, M. D. Permana, L. K. Sakti, G. A. N. Sheha, Solihudin, S. Hidayat, T. Takei, N. Kumada, I. Rahayu, *Nanomaterials* **2023**, *13*, 704.
- [10] T. M. Khedr, S. M. El-Sheikh, A. Hakki, A. A. Ismail, W. A. Badawy, D. W. Bahnemann, *J. Photochem. Photobiol. Chem.* **2017**, *346*, 530–540.
- [11] F. Cao, J. Xiong, F. Wu, Q. Liu, Z. Shi, Y. Yu, X. Wang, L. Li, *ACS Appl. Mater. Interfaces* **2016**, *8*, 12239–12245.
- [12] M. M. Mohamed, B. H. M. Asghar, H. A. Muathen, *Catal. Commun.* **2012**, *28*, 58–63.

- [13] K. Fischer, A. Gawel, D. Rosen, M. Krause, A. Abdul Latif, J. Griebel, A. Prager, A. Schulze, *Catalysts* **2017**, *7*, 209.
- [14] G. Xiang, Y.-G. Wang, J. Li, J. Zhuang, X. Wang, *Sci. Rep.* **2013**, *3*, 1411.
- [15] D. Tsukamoto, Y. Shiraishi, Y. Sugano, S. Ichikawa, S. Tanaka, T. Hirai, *J. Am. Chem. Soc.* **2012**, *134*, 6309–6315.
- [16] Q. Shi, X. Zhang, Z. Li, A. Raza, G. Li, *ACS Appl. Mater. Interfaces* **2023**, *15*, 30161–30169.
- [17] J. Wang, Z. Wang, W. Wang, Y. Wang, X. Hu, J. Liu, X. Gong, W. Miao, L. Ding, X. Li, *Nanoscale* **2022**, *14*, 6709–6734.
- [18] O. M. Lavrynenko, M. M. Zahornyi, E. Paineau, O. Y. Pavlenko, N. I. Tyschenko, O. I. Bykov, *Mater. Today Proc.* **2022**, *62*, 7664–7669.
- [19] O. M. Lavrynenko, M. M. Zahornyi, O. Y. Pavlenko, A. I. Bykov, *Appl. Nanosci.* **2023**, *13*, 5115–5124.
- [20] O. M. Lavrynenko, M. M. Zahornyi, E. Paineau, P. O. Yu, *Appl. Nanosci.* **2023**, 1–13.
- [21] K. M. Mayya, N. Jain, A. Gole, D. Langevin, M. Sastry, *J. Colloid Interface Sci.* **2004**, *270*, 133–139.
- [22] P. Nyamukamba, L. Tichagwa, O. Okoh, L. Petrik, *Mater. Sci. Semicond. Process.* **2018**, *76*, 25–30.
- [23] L. Brohan, A. Verbaere, M. Tournoux, G. Demazeau, *Mater. Res. Bull.* **1982**, *17*, 355–361.
- [24] W. Hu, Y. Liu, R. L. Withers, T. J. Frankcombe, L. Norén, A. Snashall, M. Kitchin, P. Smith, B. Gong, H. Chen, *Nat. Mater.* **2013**, *12*, 821–826.
- [25] C. Wang, J. Li, E. Paineau, A. Laachachi, C. Colbeau-Justin, H. Remita, M. N. Ghazzal, *J. Mater. Chem. A* **2020**, *8*, 10779–10786.
- [26] B. Erdem, R. A. Hunsicker, G. W. Simmons, E. D. Sudol, V. L. Dimonie, M. S. El-Aasser, *Langmuir* **2001**, *17*, 2664–2669.
- [27] K. Wang, Z. Bielan, M. Endo-Kimura, M. Janczarek, D. Zhang, D. Kowalski, A. Zielińska-Jurek, A. Markowska-Szczupak, B. Ohtani, E. Kowalska, *J. Mater. Chem. A* **2021**, *9*, 10135–10145.
- [28] N. Li, P. Zhao, D. Astruc, *Angew. Chem. Int. Ed.* **2014**, *53*, 1756–1789.
- [29] P. Jimenéz-Calvo, M. J. Muñoz-Batista, M. Isaacs, V. Ramnarain, D. Ihiwakrim, X. Li, M. Á. Muñoz-Márquez, G. Teobaldi, M. Kociak, E. Paineau, *Chem. Eng. J.* **2023**, *459*, 141514.
- [30] J. Zhang, H.-D. Wang, Y. Zhang, Z. Li, D. Yang, D. H. Zhang, T. Tsukuda, G. Li, *J. Phys. Chem. Lett.* **2023**, *14*, 4179–4184.
- [31] W. Spencer, J. R. Sutter, *J. Phys. Chem.* **1979**, *83*, 1573–1576.
- [32] V. A. Solé, E. Papillon, M. Cotte, P. Walter, J. Susini, *Spectrochim. Acta Part B At. Spectrosc.* **2007**, *62*, 63–68.

The synthesis of Au-doped TiO<sub>2</sub> nanocomposites is carried out by a chemical co-deposition method with glucose used as reducing agent of gold. Structural characterizations confirm that Au is dispersed homogeneously into the nanocomposites, inducing a progressive shift of both valence and conduction band edges. Adsorption and photodegradation performance are assessed as a function of the nature of the dye.

O. M. Lavrynenko,\* M. M. Zahornyi,\* O. Y. Pavlenko, C. Hotton, J. Bodin, V. D. Quach, M. N. Ghazzal, and E. Paineau\*

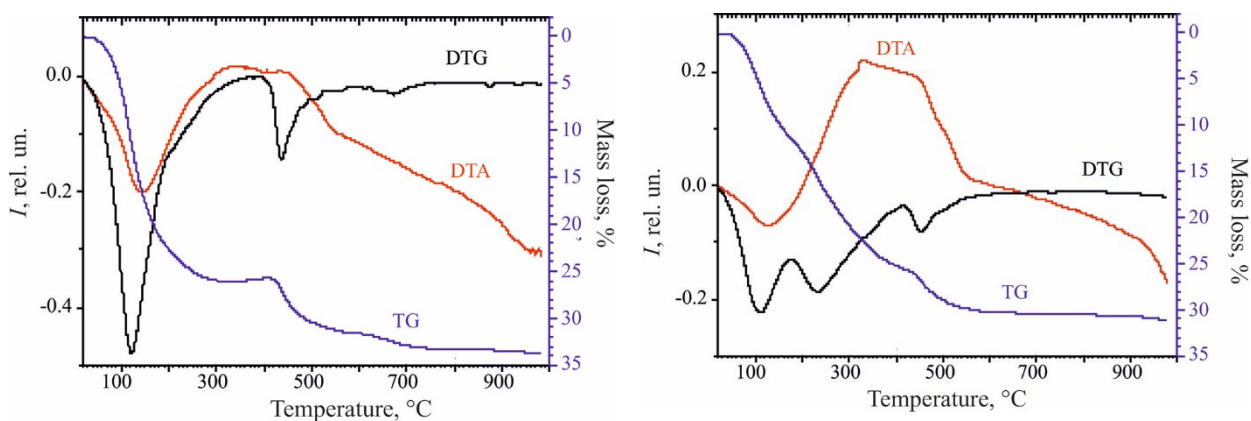
### Structural Properties and Photocatalytic Activity of TiO<sub>2</sub>/Au Nanocomposites Synthesized with Glucose



## Supporting Information

**Structural Properties and Photocatalytic Activity of TiO<sub>2</sub>/Au Nanocomposites Synthesized with Glucose**

*Olena M. Lavrynenko,\* Maksym M. Zahornyi,\* Olesya Y. Pavlenko, Claire Hotton, Jennifer Bodin, Vien-Duong Quach, Mohamed Nawfal Ghazzal, and Erwan Paineau\**

**1. Thermogravimetric analyses**

**Figure S1.** Thermogravimetric (TG, blue curves), differential thermogravimetric (DTG, dark curves) and differential thermal analysis (DTA, red curves) of the titanium (IV) isopropoxide precipitates doped with gold at (*left*) 0.5 and (*right*) 3.5 wt.%.

## 2. Crystal lattice parameters

**Table S1.** Crystal lattice parameters of TiO<sub>2</sub> phases doped with gold.

Sample code	Lattice parameters (nm)		c/a	d <sub>101</sub> (nm)
	a	c		
TiO <sub>2</sub> /Au_0.5	0.3761	0.9569	2.54	0.35004
TiO <sub>2</sub> /Au_1	0.3745	0.9612	2.57	0.35111
TiO <sub>2</sub> /Au_3	0.3772	0.9957	2.64	0.35049
TiO <sub>2</sub> /Au_3.5	0.3732	0.9512	2.55	0.34742

## 3. Morphology of the nanocomposites

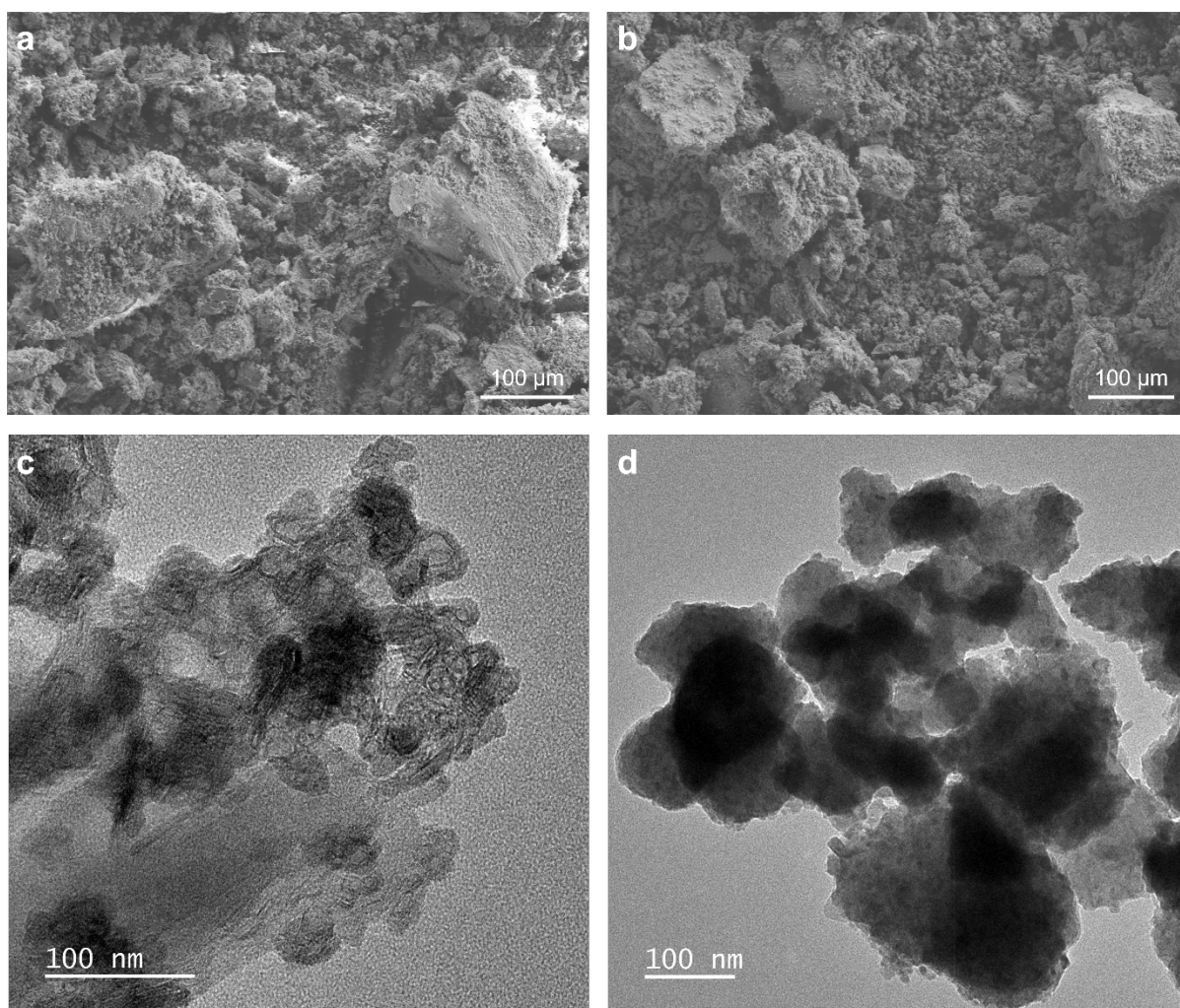


**Figure S2.** (a,b) Scanning and (c,d) transmission electron microscopy images of TiO<sub>2</sub>/Au nanocomposites prepared with gold at (a,c) 0.5 and (b,d) 3.5 wt.%.

## 4. X-ray fluorescence spectroscopy

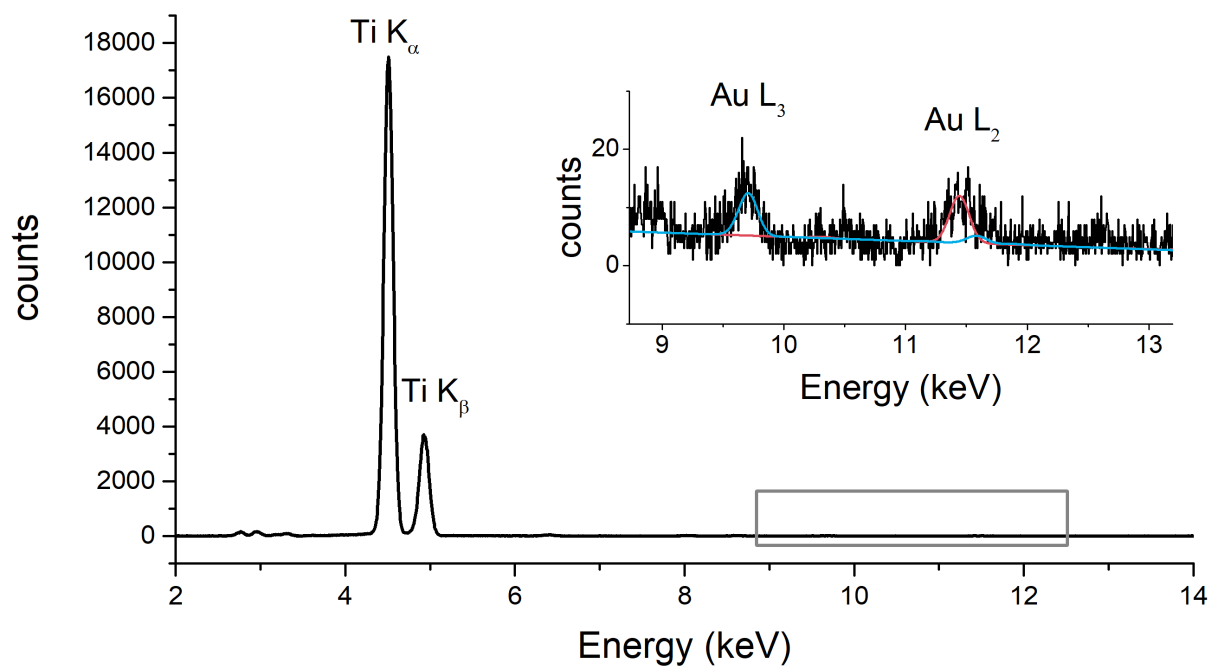


**Figure S3.** X-ray fluorescence spectra obtained on TiO<sub>2</sub>/Au<sub>0.5</sub> nanocomposite. The inset is a zoom of the grey rectangle, corresponding to the L<sub>3,2</sub> fluorescence peak of gold (Au). The colored lines represent the fit of the Au contribution.

## 5. X-ray photoelectron spectroscopy

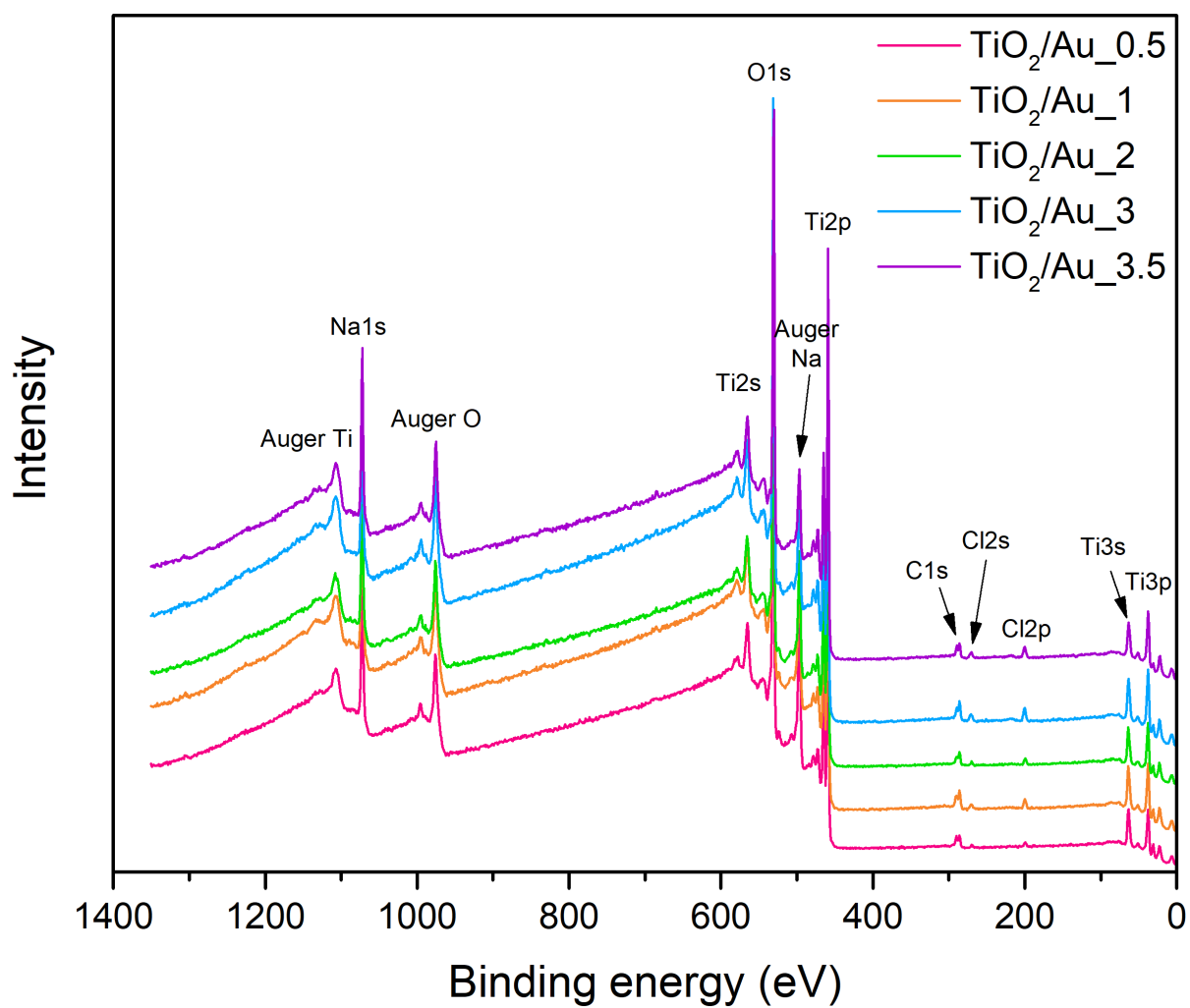


**Figure S4.** Survey XPS spectra of the different TiO<sub>2</sub>/Au nanocomposites.